



FULL LENGTH ARTICLE

All-trans retinoic acid inhibits the malignant behaviors of hepatocarcinoma cells by regulating ferroptosis

Yanting Sun ^{a,1}, Yun He ^{b,1}, Jishuang Tong ^a, Daijiang Liu ^c,
Haodong Zhang ^a, Tongchuan He ^d, Yang Bi ^{a,*}

^a Stem Cell Biology and Therapy Laboratory, Children's Hospital of Chongqing Medical University, National Clinical Research Center for Child Health and Disorders, Ministry of Education Key Laboratory of Child Development and Disorders, Chongqing Key Laboratory of Pediatrics, Chongqing 400014, PR China

^b Department of Pediatric Surgery, Children's Hospital of Chongqing Medical University, Chongqing 400014, PR China

^c Department of Gastroenterology, Chongqing Emergency Medical Centre, Chongqing 400014, PR China

^d Molecular Oncology Laboratory, Department of Surgery, The University of Chicago Medical Centre, Chicago, IL 60637, USA

Received 29 November 2021; accepted 12 April 2022

Available online 5 May 2022

KEYWORDS

All-trans retinoic acid;
Ferroptosis;
Hepatocarcinoma;
Invasion;
Migration

Abstract All-trans retinoic acid (ATRA) can reverse the malignant behaviors of hepatocellular carcinoma (HCC) cells, thereby exerting anti-HCC effect; however, the underlying mechanism is yet to be understood. This study aimed to demonstrate that ATRA is vital to ferroptosis in HCC. Ferroptosis-related genes exhibit different expression in patients with HCC compared to that in healthy individuals. A total of 20 amino acid products were detected in HepG2 cells, the expression level of 5 was decreased after ATRA treatment. ATRA improved the levels of lipid ROS, MDA, and $\text{NAPD}^+/\text{NADPH}$, and reduced the mt-DNA copy number and changed the structure of mitochondria, in HepG2 and Hep3B cells. We found the expression of genes positively correlated with ferroptosis to increase and those negatively correlated to decrease with

Abbreviations: ATRA, all-trans-retinoic acid; ROS, reactive oxygen species; SOD1, superoxide dismutase 1; GPX4, glutathione peroxidase 4; HO-1, heme oxygenase 1; NQO-1, NAD(P)H quinone dehydrogenase 1; CAT, catalase; GCLC, glutamate-cysteine ligase catalytic subunit; ND1, NADH dehydrogenase subunit 1; DCFH-DA, 2,7-dichlorofluorescein diacetate; FTH1, ferritin heavy chain 1; TFRC, transferrin receptor; ACSL4, acyl-CoA synthetase long chain family member 4; SLC7A11, solute carrier family 7 member 11; SLC3A2, solute carrier family 3 member 2; MDA, malondialdehyde; Fer-1, Ferrostatin-1; ICG, indocyanine; PAS, periodic acid-schiff.

* Corresponding author. Stem Cell Biology and Therapy Laboratory, Children's Hospital of Chongqing Medical University, Building 7, Room 905, 136 Zhongshan Er Road, Chongqing 400014, PR China.

E-mail address: yang_bi@hospital.cqmu.edu.cn (Y. Bi).

Peer review under responsibility of Chongqing Medical University.

¹ Contributed equally.

<https://doi.org/10.1016/j.gendis.2022.04.011>

2352-3042/Copyright © 2022, Chongqing Medical University. Production and hosting by Elsevier B.V. This is an open access article under the CC BY-NC-ND license (<http://creativecommons.org/licenses/by-nc-nd/4.0/>).

ATRA treatment. Inhibition of ferroptosis by Ferrostatin-1 reversed ATRA-inhibited proliferation of HCC cells, along with cell migration and invasion. GSH synthesis was blocked by ATRA, accompanied by decreased cystine content and increased glutamate content, and downregulation of the expression of GSH synthesis-related genes. Our findings suggested that ATRA inhibited the malignancy of HCC cells by improving ferroptosis, and that inhibition of GSH synthesis contributed to ATRA-induced ferroptosis.

Copyright © 2022, Chongqing Medical University. Production and hosting by Elsevier B.V. This is an open access article under the CC BY-NC-ND license (<http://creativecommons.org/licenses/by-nc-nd/4.0/>).

Introduction

Hepatocellular carcinoma (HCC) is one of the most common malignant tumors, with third highest mortality rate in the world. It is an important health issue in China, the number of patients with HCC in China accounts for approximately 45% of cases across the world.^{1–3} Although partial hepatectomy or liver transplantation can significantly improve the survival rate of patients with HCC, most patients are diagnosed at middle-late stage, when the opportunity of surgery is already lost. The prognosis of HCC still remains poor, and is inextricably linked to its high recurrence and frequent metastases.^{4,5} Therefore, recent studies on HCC have mainly focused on how to effectively control its rapid growth and prevent its metastasis.^{6,7}

All-trans retinoic acid (ATRA) is an active form of retinoic acid, which can regulate the growth and differentiation of normal and malignant cells by binding to retinoic acid receptors (RARs/RXRs).⁸ We had previously shown that ATRA inhibits the proliferation, migration, and metastasis of HCC cells by reversing epithelial–mesenchymal transition (EMT), thereby implying its potential clinical application in HCC treatment. However, the molecular mechanism of ATRA in HCC is not completely clear.^{9,10}

Ferroptosis is a new type of cell death, characterized by lipid peroxidation. Under the action of divalent iron or ester oxygenase, unsaturated fatty acids express largely on the cell membrane to produce lipid peroxidation and induce cell death.¹¹ Ferroptosis has been associated with many diseases, such as neurotoxicity/neurodegenerative diseases, ischemia reperfusion injury, and tumors.^{12,13} Sorafenib is an effective chemotherapeutic drug against HCC, and plays cytotoxic role by inducing ferroptosis; therefore, ferroptosis may be a potentially effective goal for the induction of cell death in HCC.¹⁴ Ferroptosis has been reported to occur during ATPR (a novel ATRA) treatment of acute myeloid leukemia,¹⁵ suggesting the possible relationship between ATRA and ferroptosis.

The current study aimed to explore whether the regulation of malignancy of HCC cells by ATRA is related to ferroptosis. We demonstrated that ATRA treatment could improve the reactive oxygen species (ROS) level in HCC cells. Ferrostatin-1 (Fer-1), a selective inhibitor of ferroptosis, reversed ATRA-inhibited malignancy of HCC cells. ATRA increased ferroptosis by regulating two subunits of glutamate-cysteine ligase modifier subunit (GCL) and cystine/glutamate transporter system xc-. Collectively, our

findings could provide a theoretical basis for understanding the anti-HCC effect of ATRA and its potential clinical application in HCC treatment.

Materials and methods

Patients and datasets

TCGA database (including 50 normal liver samples and 374 HCC samples) and GSE36376 database (including 193 normal liver samples and 240 HCC samples) were used for identification of the differentially expressed genes (DEGs) and further analysis. TCGA database was analyzed by DESeq2 and GSE36376 database was analyzed by limma package. $Padj < 0.05$ and $|\log_2\text{FoldChange}| > 0.5$ were considered to be significant. To explore the interactions between these genes, Protein–Protein Interaction (PPI) network was constructed by using the STRING online platform (<http://www.cn.string-db.org>) to explore the interactions between these DEGs. Gene Ontology (GO) and Kyoto Encyclopedia of Genes and Genomes (KEGG, <http://www.genome.jp>) analyses were performed by using clusterProfiler package to analyze the expression characteristics and biological function of DEGs.

Metabolites detection

HepG2 were treated with 10 $\mu\text{mol/L}$ of ATRA for 48 h. Metabolites between control and ATRA groups were determined by LC-MS/MS (MetWare, Wuhan, China). The difference of amino acid metabolites was presented as heatmap. $|\log_2\text{FoldChange}| > 1$ was considered to be significant.

Cell culture and treatment

Two types of human hepatocarcinoma cell line HepG2 and Hep3B were purchased from the ATCC (Manassas, USA). Cells were cultured in DMEM (Gibco, Carlsbad, USA) supplied with 10% FBS (Gibco, Carlsbad, USA), at 37 °C with 5% CO₂. Hepatocarcinoma cells were divided into three groups: control group, ATRA group (treated with 10 $\mu\text{mol/L}$ of ATRA, Sigma Aldrich, St. Louis, USA), ATRA + Fer-1 (Sigma Aldrich, St. Louis, USA) group (treated with 10 $\mu\text{mol/L}$ of ATRA and 1 $\mu\text{mol/L}$ of Fer-1).

Detection of Fe²⁺

HCC cells were seeded in a 60-mm dish with different treatments for 48 h. The cell supernatant was discarded and the FerroOrange (1 μmol/L, Dojindo, Japan) solution was added to the cells for 40 min at 37 °C. The content of Fe²⁺ was detected by flow cytometry (BD FACSCanto II, New Jersey, USA) and the distribution of Fe²⁺ was observed under laser confocal microscope (Nikon, Tokyo, Japan). Each experiment was repeated at least three times.

Detection of total ROS and lipid ROS

Cells were incubated with DCFH-DA (10 μmol/L, Beyotime, Shanghai, China) at 37 °C for 30 min. Cells were then subjected to flow cytometry analysis for ROS detection. To detect intracellular lipid ROS, cells were incubated with C11-BODIPY (50 μmol/L, Thermo Fisher Scientific, Inc., MA, USA) at 37 °C for 1 h. Excess C11-BODIPY was removed by washing cells twice with PBS. Lipid ROS is proportional to the oxidation of polyunsaturated butadienyl portion of C11-BODIPY. When cells are oxidized, the released lipid ROS quench the originally red fluorescence and elicit green fluorescence under confocal microscope.

GSH/GSSG, MDA, cystine and glutamate content assay

HCC cells were seeded in a 100-mm dish with different treatments for 48 h. Cell lysates were collected, the level of reduced glutathione (GSH), oxidized glutathione disulfide (GSSG), malondialdehyde (MDA), cystine and glutamate was detected according to the manufacturer's instructions (Solarbio, Beijing, China).

Transmission electron microscopy (TEM) detection

After 48 h of treatment, HCC cells were digested and cell pellet was obtained with centrifuge at 1000 g for 10 min. The pellet samples were subsequently fixed, rinsed, dehydrated, soaked and embedded. The ultrathin sections were captured by TEM in the electron microscope laboratory of the Institute of Life Sciences, Chongqing Medical University.

Real-time PCR analysis

Total RNA in all groups was extracted with RNA Extraction kit (Biotek, Beijing, China); the concentration and purity of RNA samples were detected at an absorbance ratio of 260/280 nm. A total of 1 μg RNA was reverse transcribed into cDNA by using Superscript II reverse transcription kit (Takara, Dalian, China). Primers (Table 1) were designed by using the Primer 3.0 program. The gene expression was quantified by using the SYBR Green qPCR Supermix kit (Invitrogen, Carlsbad, CA, USA). The relative level of mRNA expression of a gene was normalized with the expression of *β-actin*.

Table 1 List of real-time PCR Primer Sequences.

Gene	Primer sequence (5'–3')
<i>human ACTB</i> (<i>β-actin</i>)	Fwd: CCTGGCACCCAGCACAAAT Rev: GGGCCGGACTCGTCATAC
<i>human ACSL4</i>	Fwd: CCAAGTAGACCAACGCCTTCAGAC Rev: TCGGTCCCAGTCCAGGTATTCTTTC
<i>human FTH1</i>	Fwd: CCATCAACCGCCAGATCAACCTG Rev: GTTCTCAGCATGTTCCCTCTCCTC
<i>human GCLC</i>	Fwd: TTGATTGTCGCTGGGGAGTGATTTC Rev: TTGTTCTCAATGGCTCCAGTCCCTC
<i>human GCLM</i>	Fwd: GCCTGTTTCAGTCTTGGAGTTGC Rev: CCTCCCAGTAAGGCTGTAAATGCTC
<i>human GPX4</i>	Fwd: CCGCTGTGGAAGTGATGAAGATC Rev: CTTGTCGATGAGGAAGTGTGGAGAG
<i>human mt-ND1</i>	Fwd: CGATTCCGCTACGACCACTCATAC Rev: GCTGGAGATTGTAATGGGTATGGAGAC
<i>human TFRC</i>	Fwd: GCTGGAGACTTTGGATCGGTTGG Rev: TATACAACAGTGGGCTGGCAGAAAC
<i>human SLC3A2</i>	Fwd: TGGGTTCCAGGTTCCGGACATAG Rev: TCTGCTGAAGGTCGGAGGAGTTAG
<i>human SLC7A11</i>	Fwd: ACGGTGGTGTGTTTGTCTGCTC Rev: GCTGGTAGAGGAGTGTGCTTGC

Mitochondrial DNA copy number

The genomic DNA was extraction by gDNA Assay Kit (AG, China), then conduct real-time PCR procedure. The mitochondrial DNA (*mt-ND1*) to nuclear DNA (*β-actin*) ratio was calculated as the mt-DNA copy number.

Western blot analysis

Cells with different treatments were lysed in RIPA buffer to collect proteins. 20 μg protein was separated on 10% SDS-PAGE gel (Beyotime, Shanghai, China) and subsequently transferred to polyvinylidene fluoride membranes (Millipore, Billerica, MA, USA). Then the membranes were blocked in the Quick-Block blocking buffer (Beyotime, Shanghai, China) for 15 min, and then incubated overnight at 4 °C with a primary antibody of heme oxygenase-1 (HO-1, 384541, ZEN-BIOSCIENCE, Chengdu, China), NAD(P)H quinone oxidoreductase 1 (NQO-1, R27096, ZEN-BIOSCIENCE, Chengdu, China), glutamate-cysteine ligase catalytic subunit (GCLC, ET1704-38, HuaBio, Zhejiang, China), glutamate-cysteine ligase modifier subunit (GCLM, ET1705-87, HuaBio, Zhejiang, China), glutathione peroxidase 4 (GPX4, ET1706-45, HuaBio, Zhejiang, China), Catalase (CAT, ET1703-31, HuaBio, Zhejiang, China), Superoxide dismutase-1 (SOD-1, ET1706-49, HuaBio, Zhejiang, China), Transferrin receptor (TFRC, ET1702-06, HuaBio, Zhejiang, China), Ferritin Heavy Chain (FTH1, ET1705-55, HuaBio, Zhejiang, China), solute carrier family 3 member 2 (SLC3A2, ER65634, HuaBio, Zhejiang, China), solute carrier family 7 member 11 (SLC7A11, 382036, ZEN-BIOSCIENCE, Chengdu, China), nuclear factor E2-related factor 2 (NRF2, 16396-1-AP, Proteintech, Wuhan, China) and *β-actin* (TA-09, ZSGB-BIO, Beijing, China). After being washed by TBST, the

membranes were incubated with appropriate second antibody (ZSGB-BIO, Beijing, China) at room temperature for 2 h and visualized by using enhanced chemiluminescent substrate (Bio-Rad, CA, USA) under the ChemiDoc Touch Imaging System (Bio-Rad, CA, USA).

Cell apoptosis assay

Cell apoptosis was determined by using Hoechst staining. In Hoechst staining assay, cells were fixed in 4% paraformaldehyde at room temperature for 30 min, and stained with Hoechst 33258 (Solarbio, Shanghai, China) for 10 min and observed under a fluorescence microscope (Nikon, Tokyo, Japan).

Wound-healing assay

HCC cells were seeded into 6-well plates with different treatments as above described. When cell confluence reached to 100% confluent monolayer after 48 h, a consistent linear wound in the surface of confluent cells was scratched with a pipette tip. After washed with PBS, cells were continuously incubated with different treatments. Bright-field images of the same wound field were captured at 0, 1, 2, 3 days to calculate the wound healing rate. The assay was independently repeated three times in triplicate.

Transwell assay for cell invasion

After 48 h of different treatments, cells of each group were resuspended in serum-free DMEM and then 200 μ L cell suspension (migration: 3×10^4 /well and invasion: 1×10^5 /well) was replanted into the upper chamber of Transwell insert (8.0 μ m, Corning, NY, USA). DMEM supplied with 10% FBS was added into the lower chamber. After 48 h of incubation with different treatments, cells were fixed for 30 min and stained with 0.1% crystal violet (Beyotime, Shanghai, China) for 20 min. After wiped away cells at the upper surface of chamber, Transwell insert was photographed, at least five independent fields of view were quantified under a light microscope (Nikon, Tokyo, Japan). The procedure was independently performed for three times with triplicate.

Periodic Acid-Schiff (PAS) staining and Indocyanine (ICG) uptake

HCC cells were seeded in 6-well plate with 10 days of different treatments, and the medium was changed every 3 days. Glycogen storage and metabolism function of mature hepatocyte were measured by PAS staining (Solarbio, Beijing, China) and ICG uptake (Sigma, St. Louis, USA) as previously described.¹⁶ Both of the procedures were performed at least three times in triplicate.

Immunofluorescence assay

HCC cells were seeded in 24-well plate with 48 h of different treatments, then fixed in 4% paraformaldehyde for 30 min, followed by permeabilized with 0.3% Triton X-

100 (Solarbio, Beijing, China) for 15 min and blocked with 5% albumin from bovine serum (Solarbio, Beijing, China) for 20 min at room temperature, followed by incubating primary antibodies against nuclear location of nuclear factor E2-related factor 2 (NRF2, 16396-1-AP, Proteintech, Wuhan, China). After gently washing with PBS, cells were subsequently incubated with appropriate secondary fluorescent antibodies (ZSGB-BIO, Beijing, China) for 1 h at room temperature. The nucleus was stained with Hoechst 33324 (Solarbio, Beijing, China). The presences of the proteins were ascertained under the laser confocal microscope (Nikon, Tokyo, Japan).

Statistical analysis

All bioinformatics results were analyzed using the R language package (version 3.62). All data were expressed as mean \pm standard deviation and analyzed using GraphPad Prism 8.0 software (GraphPad Software Inc., USA). Statistical analysis was performed by using a two-tailed Student's *t*-test to determine significant differences between two groups, while One-Way ANOVA and a post hoc SNK's test were used to measure significant differences among more than three groups. The $P < 0.05$ was considered statistically significant.

Results

Identification and enrichment analysis of ferroptosis-related DEGs

Well-defined ferroptosis-related genes were analyzed by DEseq2; 122 of them were found to be differentially expressed, as per TCGA database (<https://xena.ucsc.edu/>), and 53 were significantly correlated with ferroptosis-DEGs obtained from GSE36376 database, analyzed by limma package ($P_{adj} < 0.05$, $|\log_2\text{FoldChange}| > 0.5$, Fig. 1A). The significantly upregulated or downregulated genes ($P_{adj} < 0.05$, $|\log_2\text{FoldChange}| > 0.5$) are marked in red or blue in the volcano plot (Fig. 1B). Using the STRING online platform, we established a PPI network based on the DEGs (Fig. 1C), and found that the ferroptosis-DEGs could distinguish between HCC and normal liver samples.

To further understand the biological functions of the 53 ferroptosis-DEGs, we used GO analysis to classify them. Results (Fig. 2A) showed ferroptosis-DEGs to be primarily enriched in "response to oxidative stress". The top 8 significantly enriched KEGGs are presented in Figure 2B; the 53 ferroptosis-DEGs were found to be most related to amino acid biosynthesis. We had previously reported that ATRA inhibited proliferation, migration, and metastasis of HCC cells by reversing EMT. However, the molecular mechanism of ATRA in HCC has remained unclear. Here, we measured the expression level of amino acid metabolites in the control group and ATRA group by LC-MS/MS (Fig. 2C). Quantitative analysis showed that the content of L-alanine, L-tyrosine, L-citrulline, L-cystine, and L-ornithine hydrochloride were decreased after ATRA treatment in HepG2 cells (Fig. 2D). Overall, the results indicated that ATRA treatment affected the biosynthesis of amino acids in HCC cells.

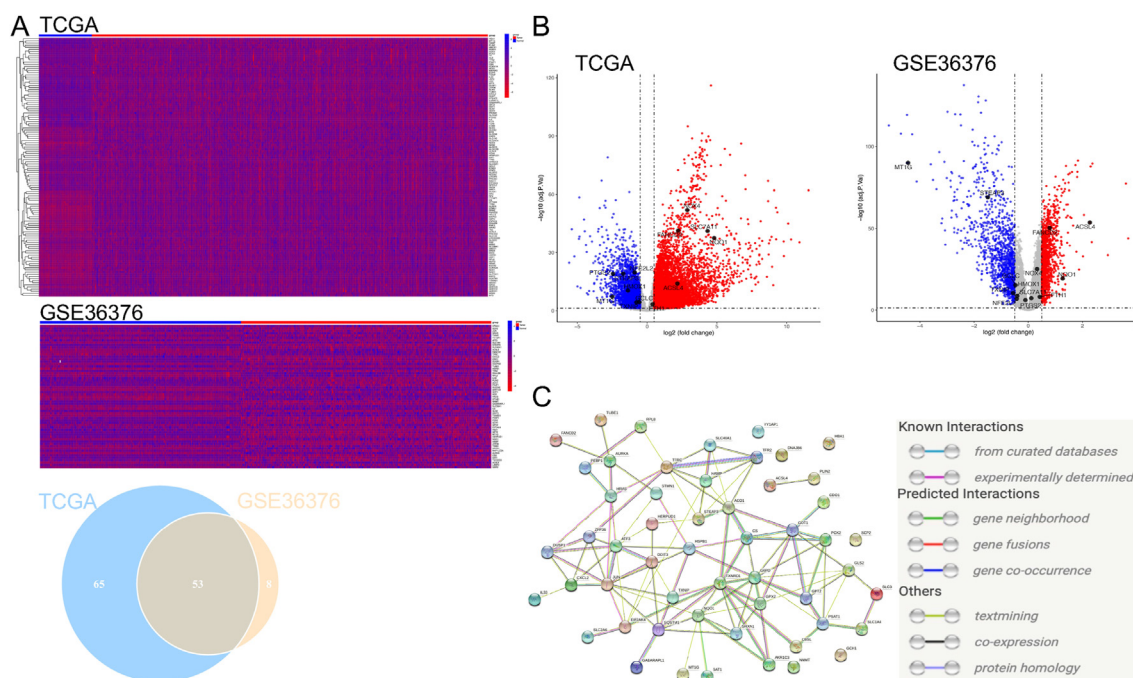


Figure 1 Identification of DEGs based on TCGA database and GSE36376 database. (A) The heatmap showed the ferroptosis related DEGs in TCGA database (374 HCC samples and 50 normal liver samples) and GSE36376 database (240 HCC samples and 193 normal liver samples), a Venn diagram was shown at below indicated that 53 DEGs were identified in the TCGA database and GSE36376 database ($P_{adj} < 0.05$, $|\log_2\text{FoldChange}| > 0.5$). (B) Volcano plot showed the significantly upregulated or down-regulated genes ($P_{adj} < 0.05$, $|\log_2\text{FoldChange}| > 0.5$) are marked in red or blue, respectively. (C) The PPI network downloaded from the STRING database indicated the interactions among the candidate genes.

ATRA treatment induced ferroptosis of HCC cells *in vitro*

To investigate whether ATRA can induce ferroptosis, we examined the level of Fe^{2+} by laser confocal microscopy and flow cytometry. Approximately 10 $\mu\text{mol/L}$ ATRA has been demonstrated to be appropriate for treating HCC cells. Compared to that in untreated cells, the content of Fe^{2+} in both HepG2 and Hep3B cells was significantly increased after 10 $\mu\text{mol/L}$ ATRA treatment (Fig. 3A); the mean fluorescence intensity of FerroOrange is shown in Figure 3B. The levels of cellular ROS and lipid ROS were also higher in ATRA group than in control group (Fig. 3C–E). The results of transmission electron microscopy showed that the mitochondria in untreated HCC cells were oval or rod-shaped, surrounded by double membrane, the inner membrane protruding inward into a flat ridge. After treatment with ATRA, the number of mitochondria decreased, they atrophied to smaller volume, and the mitochondrial ridge decreased or even disappeared (Fig. 4A). In addition, the mt-DNA copy number decreased (Fig. 4B). The results, taken together, indicated that ATRA treatment significantly increased ferroptosis in HCC cells.

ATRA treatment regulated the expression of ferroptosis-related genes of HCC cells *in vitro*

We then measured the expression of ferroptosis-related genes. Data showed that ATRA decreased the expression of *FTH1*, *GCLC*, *GCLM*, *SLC3A2*, and *SLC7A11* (suppressors that prevent ferroptosis) and increased the expression of *TFRC*

and *ACSL4* (drivers that promote ferroptosis) (Fig. 5). This finding suggested the association between ATRA and ferroptosis in HCC cells.

ATRA-induced ferroptosis in HCC cells was reversed by Fer-1

Fer-1, an inhibitor of ferroptosis, was used to verify whether ferroptosis is involved in HCC. As shown in Figure 6A and B, the high levels of cellular ROS and lipid ROS induced by ATRA were reversed upon Fer-1 treatment. Compared to that in the ATRA group, there was a significant increase in $\text{NADP}^+/\text{NADPH}$ after Fer-1 treatment (Fig. 6C). Compared to that in the control group, addition of ATRA resulted in a significant increase in lipid hyper-oxidation MDA content, which was alleviated by the addition of Fer-1 (Fig. 6D). Fer-1 also increased the mt-DNA copy number of Hep3B and HepG2 cells compared to that in ATRA group (Fig. 6E). ATRA downregulated the protein expression of *FTH1*, *GPX4*, *NQO-1*, *HO-1*, *CAT*, and *SOD-1*, and upregulated the expression of *TFRC* and *NOX4* in HCC cells, which were, however, reversed by Fer-1 treatment (Fig. 6F). The above results indicated that Fer-1 could effectively inhibit ATRA-induced ferroptosis.

ATRA-induced inhibition of HCC was reversed by Fer-1

We investigated the malignancy of HCC cells. Proliferation, migration, and invasion abilities of HepG2 and Hep3B cells were inhibited by ATRA. Colony formation (Fig. 7A) and would

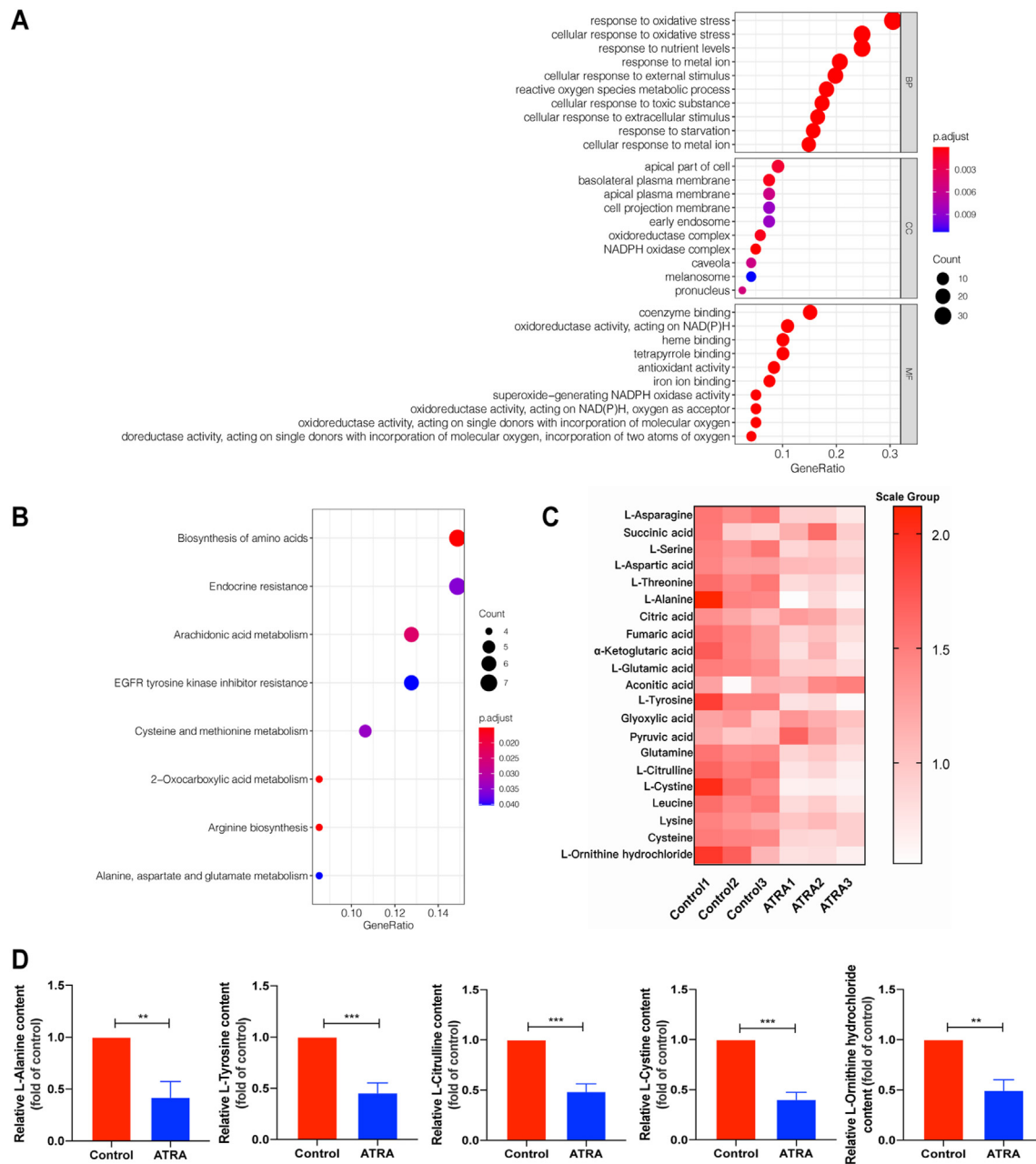


Figure 2 Enrichment Analysis of the DEGs and metabolites detection of HepaG2 cells. **(A)** GO and **(B)** KEGG analyses were detected by clusterProfiler package. **(C)** The HCA (hierarchical cluster analysis) results of metabolites in control group and ATRA group were presented as heatmaps. **(D)** The changes of metabolites between control group and ATRA group were determined by UPLC-MS/MS in HepG2 cells. $**P < 0.01$, $***P < 0.001$.

healing rate (Fig. 7B) were partly reversed with ATRA + Fer-1 treatment. Transwell assay showed ATRA-inhibited cell invasion (Fig. 7C) capability to be almost rescued by the inhibition of Fer-1. However, inhibition of Fer-1 could not affect ATRA-induced glycogen synthesis and ICG uptake (Fig. 7D) of HCC cells (Fig. 7E). No significant difference in cell apoptosis was seen between ATRA and ATRA + Fer-1 groups. Ferroptosis is a new type of cell death that differs from apoptosis; the latter was not different between ATRA and ATRA + Fer-1 groups, indicating that Fer-1 did not affect ATRA-induced cell apoptosis (Fig. 7F). The data collectively suggested that ferroptosis plays an important role in the anti-HCC effect of ATRA

by influencing the malignant behaviors of HCC cells but not their differentiation.

ATRA increased ferroptosis by regulating the synthesis of GSH

Expression and activity of system xc- and GCL are regulated by NRF2, in most cells, in response to oxidative stress. Many researches have demonstrated ATRA to be an effective NRF2 inhibitor.^{17,18} As reported earlier, NRF2 plays a role in anti-oxidative stress and anti-ferroptosis processes. Our data showed that both of total protein and nuclear protein, the

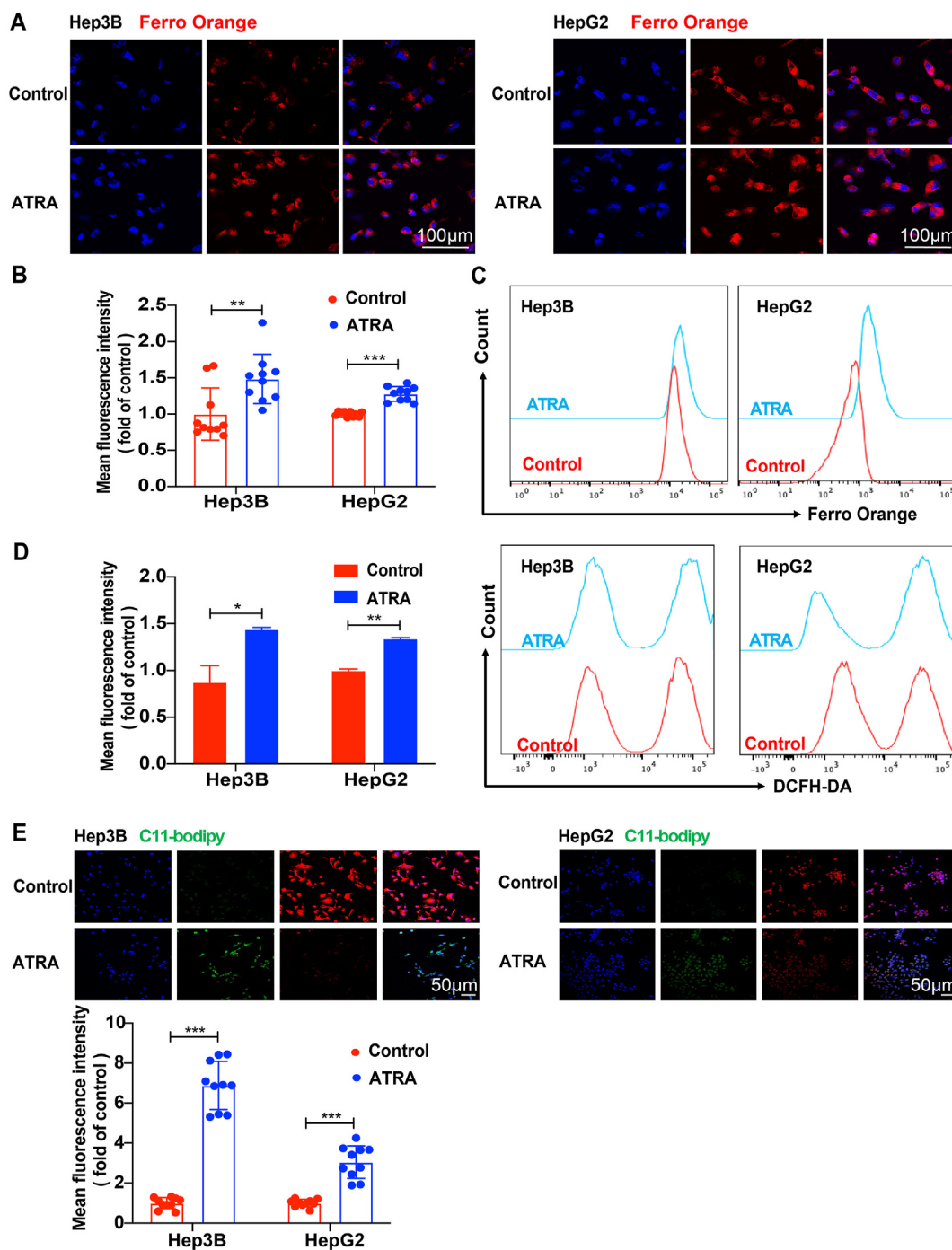


Figure 3 All-trans retinoic acid induced ferroptosis in HCC cells. HepG2 and Hep3B cells were treated with 10 $\mu\text{mol/L}$ of ATRA for 48 h. (A) The level of iron ion was measured by assay kit. (B) Mean fluorescence intensity was compared between control and all-trans retinoic acid (ATRA) treated groups. (C, D) Total reactive oxygen species (ROS) was measured by fluorescence of DCFH-DA. (E) Lipid ROS was measured by fluorescence of C11-BODIPY under confocal microscope. * $P < 0.05$, ** $P < 0.01$, *** $P < 0.001$.

active form of NRF2, were decreased after ATRA treatment, and could be reversed by Fer-1 (Fig. 8A). Compared to that in the control group, intracellular glutamate content increased and cystine content and ratio of reduced GSH/GSSG decreased in ATRA-treated groups, and the change of above amino acid content could be reversed by Fer-1 treatment (Fig. 8B). Expression of several GSH synthesis-

related proteins (GCLC, GCLM), and two subunits of the cystine-glutamate transport receptor (SLC3A2 and SLC7A11) decreased with ATRA treatment (Fig. 8C). Expression of these proteins could be reversed by Fer-1 treatment. The mRNA expression of *GCLC*, *GCLM*, *SLC3A2*, and *SLC7A11* was consistent with Western blot results (Fig. 8D). A working mode of our research is shown in Figure S1. The results

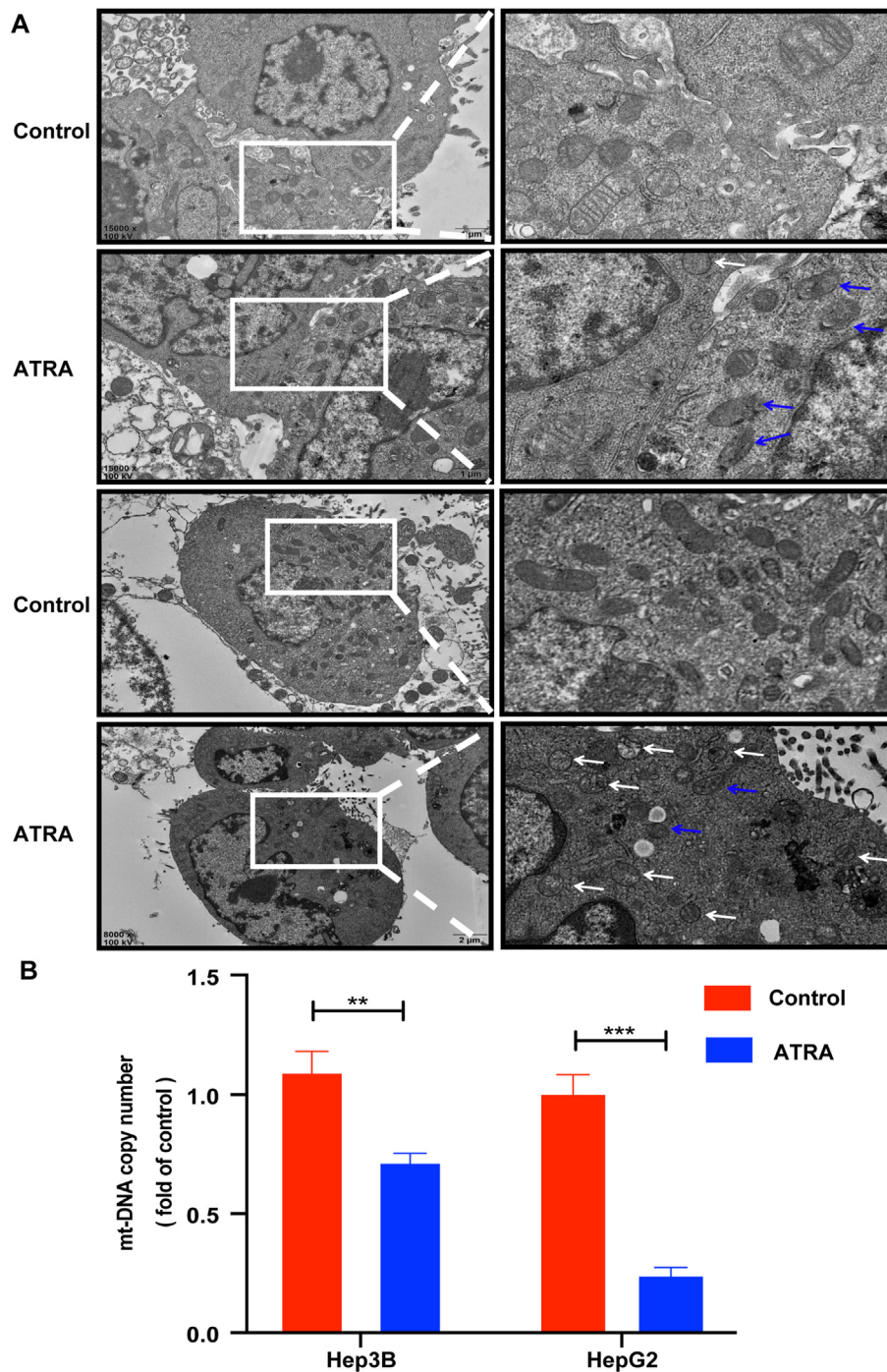


Figure 4 All-trans retinoic acid affected mitochondrion in HCC cells. (A) The mitochondrion was measured by transmission electron microscopy detection. (B) Mitochondrial DNA copy number in HCC cells decreased with all-trans retinoic acid (ATRA) treatment. $**P < 0.01$, $***P < 0.001$.

indicated that ATRA reduced the synthesis of GSH by downregulating the expression of GSH synthesis genes.

Discussion

Ferroptosis is a new mode of programmed cell death, driven by iron overload. Iron overload causes excessive total iron in

the body, which is widely deposited in the parenchymal cells of organs and tissues, often accompanied by significant proliferation of fibrous tissue, resulting in damage to the function of multiple organs.^{19,20} Liver is the main organ of iron storage, and is also the main target organ of iron overload. Excessive iron can damage DNA of liver cells, cause liver fibrosis, and promote the development of liver cancer.²¹ More than 50% of patients with liver cancer have slight iron overload and more

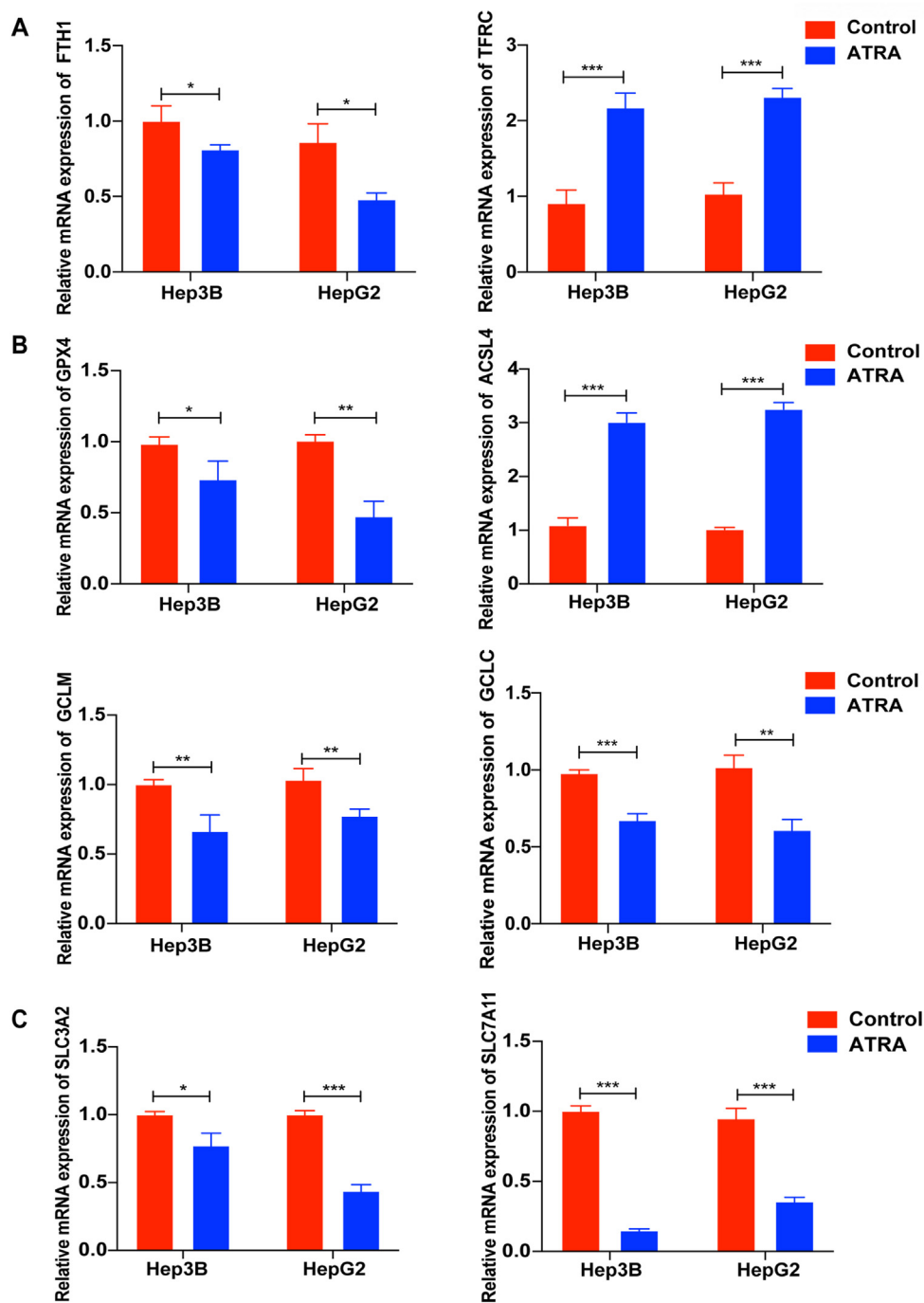


Figure 5 All-trans retinoic acid regulated the expression of ferroptosis related genes in HCC cells. HepG2 and Hepa3B cells were treated with 10 $\mu\text{mol/L}$ of all-trans retinoic acid (ATRA) for 48 h, the mRNA expression of ferroptosis related genes including *FTH1*, *TFRC*, *GPX4*, *ACSL4*, *GCLC*, *GCLM*, *SLC3A2*, and *SLC7A11* were analyzed by real-time PCR. * $P < 0.05$, ** $P < 0.01$, *** $P < 0.001$.

than 80% of ferroptosis-related genes are different between HCC and normal tissues; high expression of *GPX4*, *G6PD*, and *NQO-1* have been reported to be closely related to poor prognosis.^{22,23} In this study, we identified the DEGs between HCC samples and normal liver samples, from TCGA database and GSE36376 database, and found 53 of them to be related to ferroptosis, further indicating the important role of ferroptosis in HCC. Ferroptosis is closely regulated by intracellular signaling pathways, including amino acid metabolism, lipid

metabolism, and iron ion metabolism. Further analysis by GO categories and KEGGs showed that the 53 ferroptosis-DEGs are mostly related to biosynthesis of amino acids. Thus, we subsequently measured the change of metabolites in HCC group and ATRA group by UPLC-MS/MS. Results showed that the content of L-alanine, L-tyrosine, L-citrulline, L-cystine, and L-ornithine hydrochloride decreased after ATRA treatment, indicating that ATRA treatment affected the biosynthesis of amino acids in HepG2 cells. As reported, L-cystine

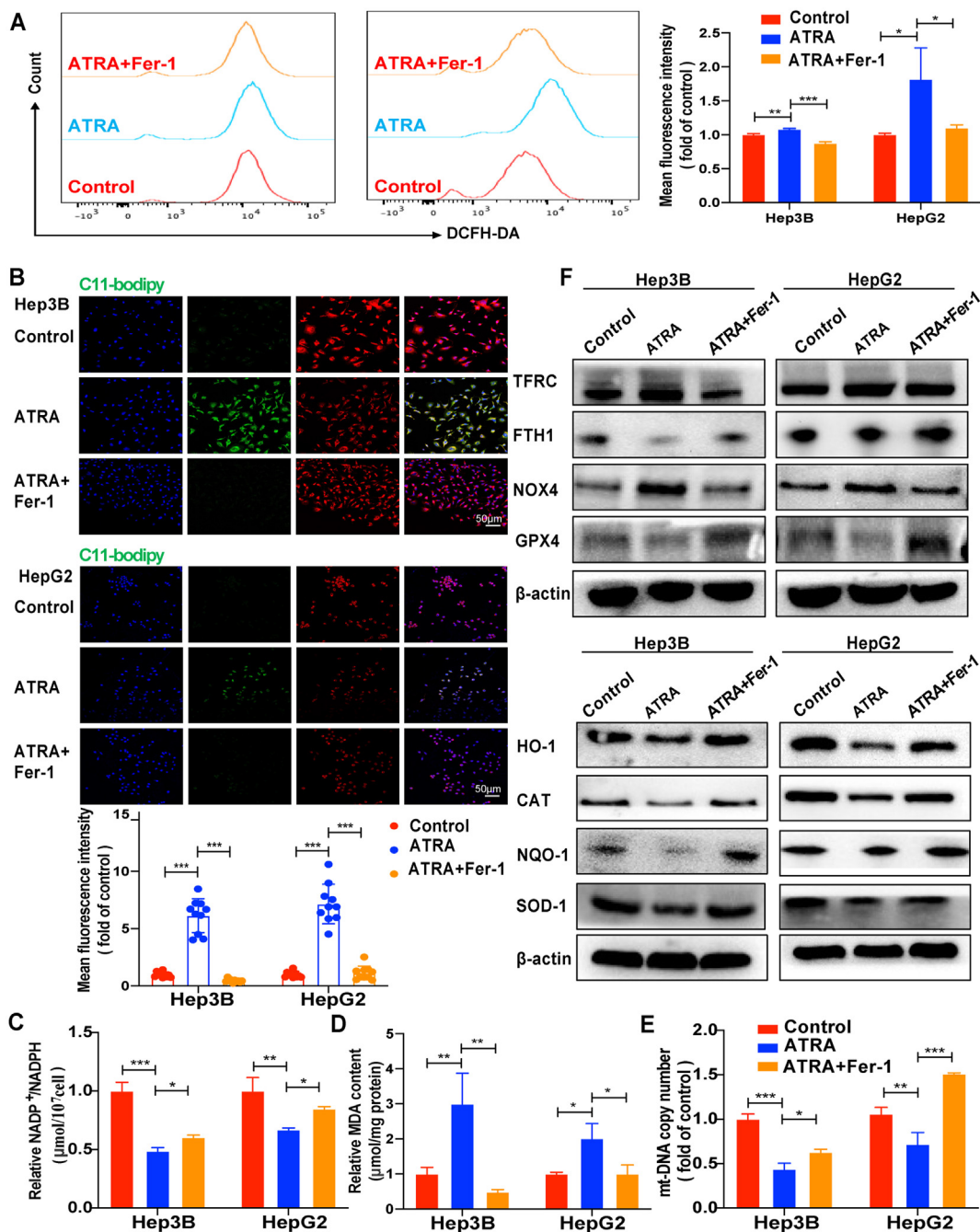


Figure 6 Ferrostatin-1 reversed all-trans retinoic acid induced ferroptosis. HepG2 and Hepa3B cells were treated with 1 μmol/L of Ferrostatin-1 (Fer-1) and 10 μmol/L of all-trans retinoic acid (ATRA) for 48 h. (A) Total reactive oxygen species (ROS) was measured by fluorescence of DCFH-DA. (B) Lipid ROS was measured by fluorescence of C11-BODIPY under confocal laser scanning microscope. (C–E) The ratio of NAD⁺/NADPH, MDA and mitochondrial DNA (mt-DNA) copy number of differently treated HCC cells. (F) Protein expression of iron metabolism related proteins were analyzed by Western blot. *P < 0.05, **P < 0.01, ***P < 0.001.

prevents damage to membrane lipids.²⁴ System xc-is an amino acid transporter widely distributed on the surface of the cell membrane, and it transports cystine into the cell with glycine and glutamate to form glutathione, a well-known antioxidant that plays an important role in scavenging ROS. Inhibition of glutamine catabolism has been reported in many literatures to cause ferroptosis.²⁵ Tyrosine is one of the amino acid residues most susceptible to oxidative modification, and its oxidation products, such as di-tyrosine (DT) and 3-

nitrotyrosine (3-NT), are biomarkers of cellular oxidative damage.²⁶ We speculate that the decrease in L-tyrosine is likely to be due to the increase of oxidative modification, but further studies are needed. Moreover, it has been reported that L-arginine has a significant protective effect on T-2 toxin-induced oxidative damage, L-arginine upregulates mRNA expressions of GSH-Px, SOD, and CAT, which are related to ferroptosis.²⁷ L-ornithine and L-citrulline are metabolites of arginine with similar effects.²⁸ Although there is no direct

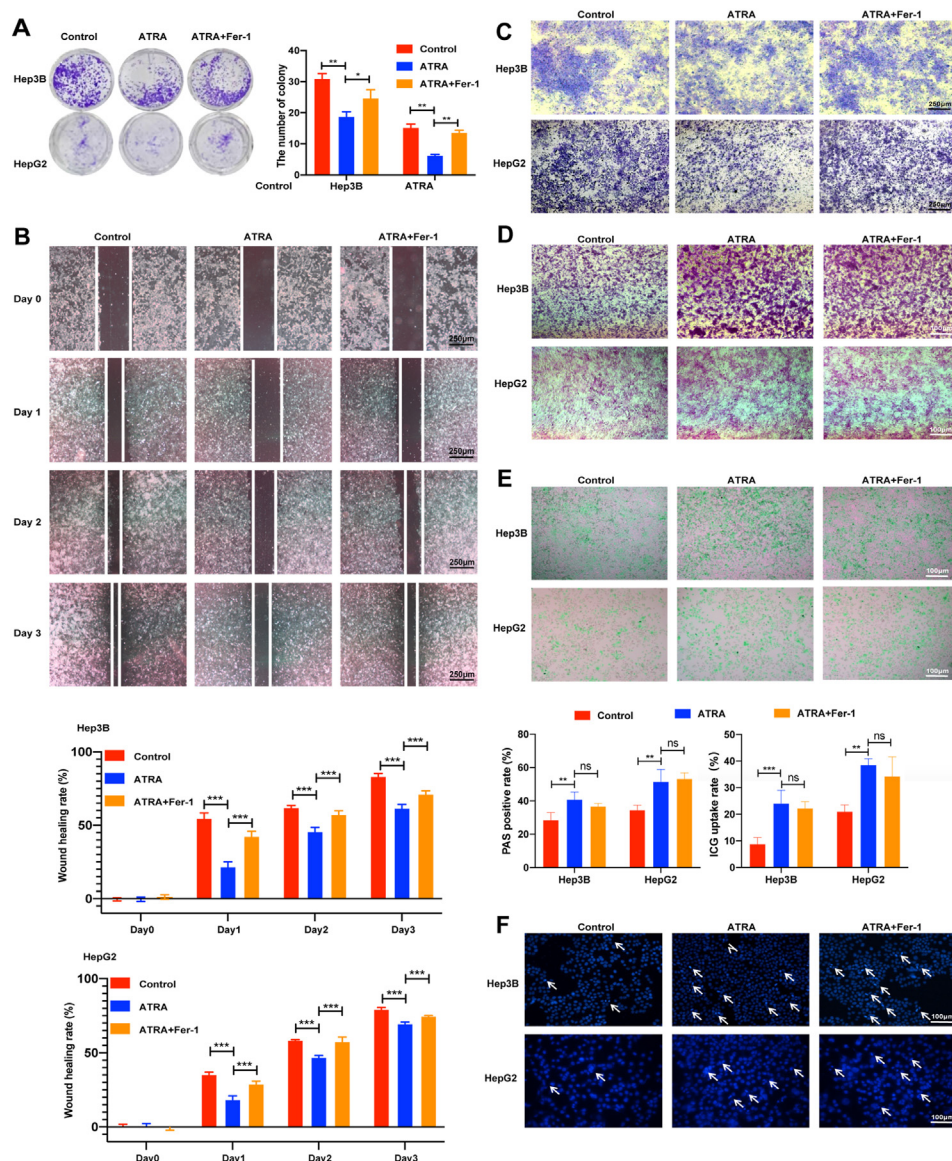


Figure 7 Ferrostatin-1 reversed the malignant behaviors of all-trans retinoic acid treated HCC cells. HepG2 and Hepa3B cells were treated with 10 $\mu\text{mol/L}$ of all-trans retinoic acid (ATRA) and 1 $\mu\text{mol/L}$ of Ferrostatin-1 (Fer-1). (A) After 14 days of culture, colony formation rate of HCC cells was measured. (B) Wound healing assay was used to detect cell migration ability. (C) Cell invasion ability was determined using a Transwell matrigel invasion assay. (D) PAS staining and (E) ICG uptake were used to detect mature function of hepatocyte. (F) Cell apoptosis was detected by Hoechst33342. ** $P < 0.01$, *** $P < 0.001$.

documentation that L-ornithine and L-citrulline inhibit ferroptosis, it is reasonable to assume that L-ornithine and L-citrulline are vital to anti-oxidative stress decrease and related to ferroptosis. Since ATRA regulates the amino acids associated with ferroptosis, the mechanism by which it regulates ferroptosis in HCC needs to be clarified.

Iron ions generate ROS and free radicals, and also participate in the regulation of ROS/free radical defense system. Therefore, excess ROS and free radicals generated by iron ions in cells can be considered to be the factors involved in cell reprogramming and carcinogenesis.^{29,30} In order to cope with the high concentration of ROS in cells, tumor cells enhance their antioxidant capacity by increasing the intracellular levels of reduced glutathione and

thioredoxin. With the adaptive evolution, tumor cells can quickly repair ROS-induced oxidatively damaged macromolecules, thereby avoiding tumor cell aging or death.^{31,32}

Sorafenib, a protein kinase inhibitor, has been approved as the first drug for systematic treatment of advanced HCC and can prolong the survival period of patients with HCC. However, drug resistance to sorafenib frequently develops during therapy of HCC.^{33,34} Sorafenib is known to affect ferroptosis in two main ways. It inhibits system xc-, leading to endoplasmic reticulum stress, GSH depletion, and iron-dependent accumulation of lipid ROS.^{35,36} Increasing reports of pathways and mechanisms related to ferroptosis in HCC, such as TP53 and Rb, suggest the anti-HCC effect of sorafenib.^{37,38} However, sorafenib fails to trigger

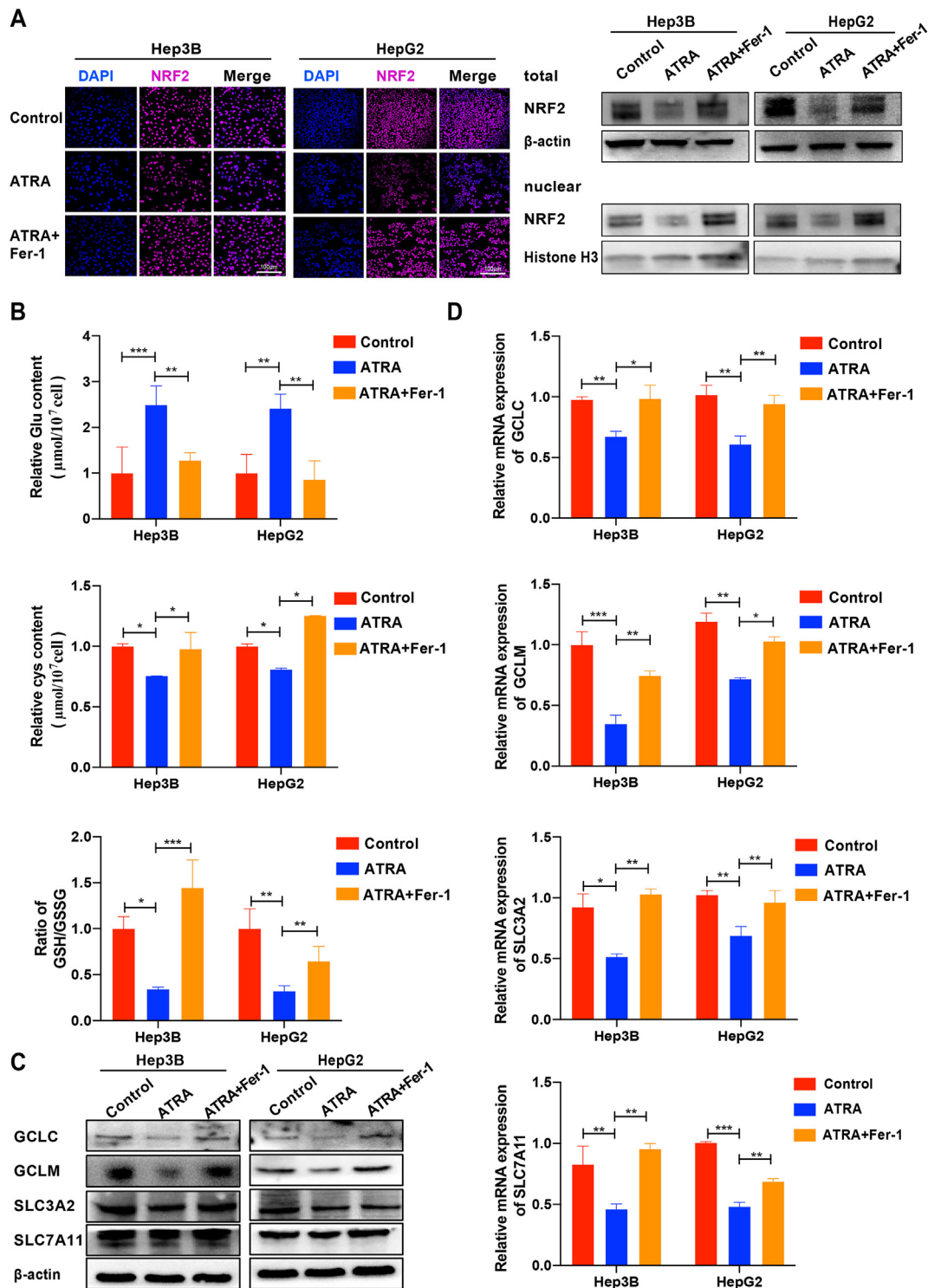


Figure 8 All-trans retinoic acid affected glutathione (GSH) synthesis by regulating nuclear factor E2-related factor 2 targets. (A) Nuclear location of nuclear factor E2-related factor 2 (NRF2) was detected by immunofluorescence and observed by confocal microscope, total protein and nuclear protein were extracted and detected by Western blot. (B) Relative cystine content, glutamate content, and the ratio of reduced glutathione/oxidized glutathione disulfide (GSH/GSSG) in different treated HCC cells. (C, D) The protein and mRNA expression of GSH synthesis related genes and proteins were detected by real-time PCR and Western blot. * $P < 0.05$, ** $P < 0.01$, *** $P < 0.001$.

ferroptosis across a wide range of cancer cell lines, implying that certain cell lines are resistant to system xc-inhibition.³⁹ In addition, sorafenib can activate p62-KEAP1-NRF2 pathway to increase NRF2, leading to an increase in reduced GSH levels, which attenuate the occurrence of ferroptosis.^{40,41} Besides of sorafenib, studies have also demonstrated the anti-HCC effect of other drugs, which can induce ferroptosis, and of new targets, which can regulate ferroptosis.^{42–44} Therefore, targeting ferroptosis can provide a new strategy for the therapy and prognosis of HCC.

ATRA could induce the cell differentiation of stem cell and tumor cell, and is widely used in the clinical treatment of acute promyelocytic leukemia. It can induce the differentiation of glioma, small cell lung cancer, and other tumor cells.^{45,46} We had previously found ATRA to inhibit the growth, migration, and invasion of HCC cells, induce differentiation and maturation in a concentration-dependent manner, by reversing EMT. However, the molecular mechanism of ATRA in HCC is not completely clear yet. Recent studies have demonstrated that ferroptosis is conducive to the inhibition of migration and invasion in human tumors.^{47,48} Our results showed that ATRA treatment resulted in the increase of intracellular iron content, lipid ROS and MDA accumulation, mitochondrial structural disorder, and the decreased number of mitochondria in HCC cells. Most of ferroptosis related genes including negative regulation genes *GPX4*, *FTH1*, *GCLC*, *GCLM*, *SOD-1* decreased,^{49,50} which also indicated that ATRA promoted ferroptosis of HCC cells. Therefore, we speculated that ATRA is likely to affect the malignant biological behaviors of HCC via the ferroptosis pathway.

Furthermore, we used a selective inhibitor, Ferrostatin-1,⁵¹ to effectively inhibit ATRA-induced ferroptosis in HCC cells, reverse the expression of ferroptosis-related genes regulated by ATRA, and decrease the levels of lipid ROS and MDA. ATRA increased the apoptosis of HCC cells; however, as a new programmed cell death, ferroptosis is distinct from apoptosis.^{11,52} We further demonstrated that Ferrostatin-1 did not affect cell apoptosis, in order to exclude the effect of apoptosis. The malignancy of cell proliferation, migration, and invasion of ATRA-induced HCC cells was rescued with the inhibition of ferroptosis. These results indicated that ATRA is likely to affect the malignant biological behaviors of HCC via the ferroptosis pathway. Further, glycogen storage and ICG metabolism function were not influenced by Fer-1, indicating that ferroptosis might not contribute to ATRA-induced differentiation of HCC cells.

NRF2 is a key transcription factor that regulates cellular response to oxidative and electrophilic stress.⁵³ NRF2 signaling pathway plays an important role in mediating lipid peroxidation and ferroptosis by controlling its target genes that prevent lipid peroxidation and free iron accumulation. Inhibition of NRF2 signal is sufficient to make tumor cells sensitive to ferroptosis.^{54,55} Most of critical glutathione synthesis and metabolism-related enzymes, such as GCL (a rate limiting enzyme for GSH synthesis),⁵⁶ glutathione synthetase (GSS), system xc-, and GPX4, all known as suppressors of ferroptosis, act under the control of NRF2.^{57,58} As an inhibitor of NRF2, ATRA down-regulates the expression of GPX4, both of the catalytic and modulatory subunits

of GCL (GCLC and GCLM), and two subunits of system xc- (SLC3A2 and SLC7A11). ATRA inhibits the transport of glutamate and cystine, resulting in the increase of glutamate content and decrease of cysteine content. Lack of raw material and reduction of glutamyl cysteine ligase inhibits the synthesis of GSH.⁵⁹ This might explain how ATRA treatment decreased the ratio of reduced GSH/GSSG, and triggered ATRA-induced ferroptosis. The pharmacological inhibition of NRF2, combined with ferroptosis inducer, can be exploited for the treatment of HCC.

Taken together, we demonstrated that ATRA treatment can promote ferroptosis in HCC cells to inhibit cell proliferation, migration, and invasion. ATRA was shown to induce ferroptosis by inhibiting GSH synthesis and strengthening lipid peroxidation, supporting its application, in combination with ferroptosis inducers, for the treatment of HCC. The opportunities and challenges of anti-HCC effect of ATRA, based on ferroptosis, as discussed here, are expected to open the way for novel strategies of HCC therapy.

Author contributions

YTS and YH performed the experiments, acquisition of the data, analysis and interpretation of the data; DJL and JST performed part of the experiments. HDZ collected and analyzed the biological information. TCH and YB were involved in the conception and design of the study and critically proof of the final manuscript, YB and YTS drafted the article. All authors read and approved the final manuscript.

Conflict of interests

Authors declare no conflict of interests.

Funding

This work was supported by a research grant from the Chongqing Science and Technology Commission (No. cstc2021jcyj-msxmX0225 to YB) and a research program of Chongqing Municipal Education Commission (No. KJQN201900442 to YB).

Data Availability

The proteome analysis data used to support the findings of this study are included within the supplementary information file.

Appendix A. Supplementary data

Supplementary data to this article can be found online at <https://doi.org/10.1016/j.gendis.2022.04.011>.

References

1. Singal AG, Lampertico P, Nahon P. Epidemiology and surveillance for hepatocellular carcinoma: new trends. *J Hepatol.* 2020;72(2):250–261.

2. Saillard C, Schmauch B, Laifa O, et al. Predicting survival after hepatocellular carcinoma resection using deep learning on histological slides. *Hepatology*. 2020;72(6):2000–2013.
3. Xie Y. Hepatitis B virus-associated hepatocellular carcinoma. *Adv Exp Med Biol*. 2017;1018:11–21.
4. Lam VW, Laurence JM, Johnston E, Hollands MJ, Pleass HC, Richardson AJ. A systematic review of two-stage hepatectomy in patients with initially unresectable colorectal liver metastases. *HPB (Oxford)*. 2013;15(7):483–491.
5. Wang JP, Yao ZG, Sun YW, et al. Clinicopathological characteristics and surgical outcomes of sarcomatoid hepatocellular carcinoma. *World J Gastroenterol*. 2020;26(29):4327–4342.
6. Zhang W, Qian S, Yang G, et al. MicroRNA-199 suppresses cell proliferation, migration and invasion by downregulating RGS17 in hepatocellular carcinoma. *Gene*. 2018;659:22–28.
7. Meng W, Chen T. Association between the HGF/c-MET signaling pathway and tumorigenesis, progression and prognosis of hepatocellular carcinoma (Review). *Oncol Rep*. 2021;46(3):191.
8. Siddikuzzaman, Guruvayoorappan C, Berlin Grace VM. All trans retinoic acid and cancer. *Immunopharmacol Immunotoxicol*. 2011;33(2):241–249.
9. Cui J, Gong M, He Y, Li Q, He T, Bi Y. All-trans retinoic acid inhibits proliferation, migration, invasion and induces differentiation of hepa1-6 cells through reversing EMT in vitro. *Int J Oncol*. 2016;48(1):349–357.
10. Fang S, Hu C, Xu L, et al. All-trans-retinoic acid inhibits the malignant behaviors of hepatocarcinoma cells by regulating autophagy. *Am J Transl Res*. 2020;12(10):6793–6810.
11. Stockwell BR, Friedmann Angeli JP, Bayir H, et al. Ferroptosis: a regulated cell death nexus linking metabolism, redox biology, and disease. *Cell*. 2017;171(2):273–285.
12. Xie Y, Hou W, Song X, et al. Ferroptosis: process and function. *Cell Death Differ*. 2016;23(3):369–379.
13. Xia X, Fan X, Zhao M, Zhu P. The relationship between ferroptosis and tumors: a novel landscape for therapeutic approach. *Curr Gene Ther*. 2019;19(2):117–124.
14. Nie J, Lin B, Zhou M, Wu L, Zheng T. Role of ferroptosis in hepatocellular carcinoma. *J Cancer Res Clin Oncol*. 2018;144(12):2329–2337.
15. Du Y, Bao J, Zhang MJ, et al. Targeting ferroptosis contributes to ATPR-induced AML differentiation via ROS-autophagy-lysosomal pathway. *Gene*. 2020;755:144889.
16. Tao L, Fang SY, Zhao L, He TC, He Y, Bi Y. Indocyanine green uptake and periodic acid-schiff staining method for function detection of liver cells are affected by different cell confluence. *Cytotechnology*. 2021;73(2):159–167.
17. Rahman ZU, Al Kury LT, Alattar A, et al. Carveol a naturally-derived potent and emerging Nrf2 activator protects against acetaminophen-induced hepatotoxicity. *Front Pharmacol*. 2021;11:621538.
18. Naeem K, Tariq Al Kury L, Nasar F, et al. Natural dietary supplement, carvacrol, alleviates LPS-induced oxidative stress, neurodegeneration, and depressive-like behaviors via the Nrf2/HO-1 pathway. *J Inflamm Res*. 2021;14:1313–1329.
19. Yun S, Chu D, He X, Zhang W, Feng C. Protective effects of grape seed proanthocyanidins against iron overload-induced renal oxidative damage in rats. *J Trace Elem Med Biol*. 2020;57:126407.
20. Brissot P, Troadec MB, Loréal O, Brissot E. Pathophysiology and classification of iron overload diseases; update 2018. *Transfus Clin Biol*. 2019;26(1):80–88.
21. Mehta KJ, Farnaud SJ, Sharp PA. Iron and liver fibrosis: mechanistic and clinical aspects. *World J Gastroenterol*. 2019;25(5):521–538.
22. Dai T, Li J, Lu X, et al. Prognostic role and potential mechanisms of the ferroptosis-related metabolic gene signature in hepatocellular carcinoma. *Pharmgenomics Pers Med*. 2021;14:927–945.
23. Tang B, Zhu J, Li J, et al. The ferroptosis and iron-metabolism signature robustly predicts clinical diagnosis, prognosis and immune microenvironment for hepatocellular carcinoma. *Cell Commun Signal*. 2020;18(1):174.
24. Ohtsu I, Kawano Y, Suzuki M, et al. Uptake of L-cystine via an ABC transporter contributes defense of oxidative stress in the L-cystine export-dependent manner in *Escherichia coli*. *PLoS One*. 2015;10(3):e0120619.
25. Luo M, Wu L, Zhang K, et al. miR-137 regulates ferroptosis by targeting glutamine transporter SLC1A5 in melanoma. *Cell Death Differ*. 2018;25(8):1457–1472.
26. Annunziata G, Jimenez-García M, Tejada S, et al. Grape polyphenols ameliorate muscle decline reducing oxidative stress and oxidative damage in aged rats. *Nutrients*. 2020;12(5):1280.
27. Yang JY, Zhang YF, Li YX, Meng XP, Bao JF. L-arginine protects against oxidative damage induced by T-2 toxin in mouse Leydig cells. *J Biochem Mol Toxicol*. 2018;32(10):e22209.
28. Shin S, Gombedza FC, Bandyopadhyay BC. L-ornithine activates Ca²⁺ signaling to exert its protective function on human proximal tubular cells. *Cell Signal*. 2020;67:109484.
29. Park JA, Park S, Park HB, Han MK, Lee Y. MUC1-C contributes to the maintenance of human embryonic stem cells and promotes somatic cell reprogramming. *Stem Cell Dev*. 2021;30(21):1082–1091.
30. Sabharwal SS, Schumacker PT. Mitochondrial ROS in cancer: initiators, amplifiers or an Achilles' heel? *Nat Rev Cancer*. 2014;14(11):709–721.
31. Harris IS, DeNicola GM. The complex interplay between anti-oxidants and ROS in cancer. *Trends Cell Biol*. 2020;30(6):440–451.
32. Mohammadalipour A, Dumbali SP, Wenzel PL. Mitochondrial transfer and regulators of mesenchymal stromal cell function and therapeutic efficacy. *Front Cell Dev Biol*. 2020;8:603292.
33. Witt-Kehati D, Fridkin A, Alaluf MB, Zemel R, Shlomai A. Inhibition of pMAPK14 overcomes resistance to sorafenib in hepatoma cells with hepatitis B virus. *Transl Oncol*. 2018;11(2):511–517.
34. Wei L, Lee D, Law CT, et al. Genome-wide CRISPR/Cas9 library screening identified PHGDH as a critical driver for Sorafenib resistance in HCC. *Nat Commun*. 2019;10(1):4681.
35. Louandre C, Ezzoukhry Z, Godin C, et al. Iron-dependent cell death of hepatocellular carcinoma cells exposed to sorafenib. *Int J Cancer*. 2013;133(7):1732–1742.
36. Li B, Wei S, Yang L, et al. C1SD2 promotes resistance to sorafenib-induced ferroptosis by regulating autophagy in hepatocellular carcinoma. *Front Oncol*. 2021;11:657723.
37. Louandre C, Marcq I, Bouhhal H, et al. The retinoblastoma (Rb) protein regulates ferroptosis induced by sorafenib in human hepatocellular carcinoma cells. *Cancer Lett*. 2015;356(2 Pt B):971–977.
38. Li Y, Xia J, Shao F, et al. Sorafenib induces mitochondrial dysfunction and exhibits synergistic effect with cysteine depletion by promoting HCC cells ferroptosis. *Biochem Biophys Res Commun*. 2021;534:877–884.
39. Zheng J, Sato M, Mishima E, Sato H, Proneth B, Conrad M. Sorafenib fails to trigger ferroptosis across a wide range of cancer cell lines. *Cell Death Dis*. 2021;12(7):698.
40. Sun X, Ou Z, Chen R, et al. Activation of the p62-Keap1-NRF2 pathway protects against ferroptosis in hepatocellular carcinoma cells. *Hepatology*. 2016;63(1):173–184.
41. Bartolini D, Dallaglio K, Torquato P, Piroddi M, Galli F. Nrf2-p62 autophagy pathway and its response to oxidative stress in hepatocellular carcinoma. *Transl Res*. 2018;193:54–71.
42. Li ZJ, Dai HQ, Huang XW, et al. Artesunate synergizes with sorafenib to induce ferroptosis in hepatocellular carcinoma. *Acta Pharmacol Sin*. 2021;42(2):301–310.
43. Zhao Y, Li M, Yao X, et al. HCAR1/MCT1 regulates tumor ferroptosis through the lactate-mediated AMPK-SCD1 activity and its therapeutic implications. *Cell Rep*. 2020;33(10):108487.

44. Shan Y, Yang G, Huang H, et al. Ubiquitin-like modifier activating enzyme 1 as a novel diagnostic and prognostic indicator that correlates with ferroptosis and the malignant phenotypes of liver cancer cells. *Front Oncol.* 2020;10:592413.
45. Christian S, Merz C, Evans L, et al. The novel dihydroorotate dehydrogenase (DHODH) inhibitor BAY 2402234 triggers differentiation and is effective in the treatment of myeloid malignancies. *Leukemia.* 2019;33(10):2403–2415.
46. Cui J, Gong M, Fang S, et al. All-trans retinoic acid reverses malignant biological behavior of hepatocarcinoma cells by regulating miR-200 family members. *Genes Dis.* 2020;8(4):509–520.
47. Huang S, Cao B, Zhang J, et al. Induction of ferroptosis in human nasopharyngeal cancer cells by cucurbitacin B: molecular mechanism and therapeutic potential. *Cell Death Dis.* 2021;12(3):237.
48. Zhu S, Yu Q, Huo C, et al. Ferroptosis: a novel mechanism of artemisinin and its derivatives in cancer therapy. *Curr Med Chem.* 2021;28(2):329–345.
49. Chen Y, Zhang P, Chen W, Chen G. Ferroptosis mediated DSS-induced ulcerative colitis associated with Nrf2/HO-1 signaling pathway. *Immunol Lett.* 2020;225:9–15.
50. Shimura T, Sharma P, Sharma GG, Banwait JK, Goel A. Enhanced anti-cancer activity of andrographis with oligomeric proanthocyanidins through activation of metabolic and ferroptosis pathways in colorectal cancer. *Sci Rep.* 2021;11(1):7548.
51. Chen C, Chen J, Wang Y, Liu Z, Wu Y. Ferroptosis drives photoreceptor degeneration in mice with defects in all-trans-retinal clearance. *J Biol Chem.* 2021;296:100187.
52. Zhang C, Zhang J, Wang J, Yan Y, Zhang C. Alpha-fetoprotein accelerates the progression of hepatocellular carcinoma by promoting Bcl-2 gene expression through an RA-RAR signalling pathway. *J Cell Mol Med.* 2020;24(23):13804–13812.
53. Sajadimajd S, Khazaei M. Oxidative stress and cancer: the role of Nrf2. *Curr Cancer Drug Targets.* 2018;18(6):538–557.
54. Dodson M, Castro-Portuguez R, Zhang DD. NRF2 plays a critical role in mitigating lipid peroxidation and ferroptosis. *Redox Biol.* 2019;23:101107.
55. Dong H, Qiang Z, Chai D, et al. Nrf2 inhibits ferroptosis and protects against acute lung injury due to intestinal ischemia reperfusion via regulating SLC7A11 and HO-1. *Aging (Albany NY).* 2020;12(13):12943–12959.
56. Song X, Long D. Nrf2 and ferroptosis: a new research direction for neurodegenerative diseases. *Front Neurosci.* 2020;14:267.
57. Zhong Q, Mishra M, Kowluru RA. Transcription factor Nrf2-mediated antioxidant defense system in the development of diabetic retinopathy. *Invest Ophthalmol Vis Sci.* 2013;54(6):3941–3948.
58. Mohar I, Botta D, White CC, McConnachie LA, Kavanagh TJ. Glutamate cysteine ligase (GCL) transgenic and gene-targeted mice for controlling glutathione synthesis. *Curr Protoc Toxicol.* 2009;Chapter 6:Unit6.16.
59. Jin Y, Huang ZL, Li L, et al. Quercetin attenuates toosendanin-induced hepatotoxicity through inducing the Nrf2/GCL/GSH antioxidant signaling pathway. *Acta Pharmacol Sin.* 2019;40(1):75–85.